(20) Lightkurve Collaboration, *Lightkurve: Kepler and TESS time series analysis in Python* (Astrophysics Source Code Library), 2018.
(21) J. M. Jenkins *et al.*, in G. Chiozzi & J. C. Guzman (eds.), *Software and Cyberinfrastructure for Astronomy IV*, *Society of Photo-Optical Instrumentation Engineers Conference Series*, **9913** (SPIE), 2016, p. 99133E.
(22) J. Southworth, P. F. L. Maxted & B. Smalley, *MNRAS*, **351**, 1277, 2004.
(23) J. Southworth, *A&A*, **557**, A119, 2013.
(24) D. Hestroffer, *A&A*, **327**, 199, 1997.
(25) P. F. L. Maxted, *A&A*, **616**, 13, 2018.
(26) J. Southworth, *The Observatory*, **143**, 71, 2023.
(27) A. Claret & J. Southworth, *A&A*, **664**, 6, 2022.
(28) A. Claret & J. Southworth, *A&A*, **674**, 7, 2023.
(29) P. F. L. Maxted *et al.*, *MNRAS*, **498**, 332, 2020.
(30) H. Ak, F. F. Özeren & F. Ekmekçi, *Information Bulletin on Variable Stars*, **5361**, 1, 2003.
(31) P. Virtanen *et al.*, *Nature Methods*, **17**, 261, 2020.
(32) J. Hübscher, *et al.*, *Information Bulletin on Variable Stars*, **5941**, 1, 2010.
(33) D. M. Popper & P. B. Etzel, *AJ*, **86**, 102, 1981.
(34) P. Lenz & M. Breger, *Communications in Asteroseismology*, **146**, 53, 2005.
(35) J. H. Telting *et al.*, *AN*, **335**, 41, 2014.
(36) A. Prša *et al.*, *AJ*, **152**, 41, 2016.
(37) J. Southworth, P. F. L. Maxted & B. Smalley, *A&A*, **429**, 645, 2005.
(38) P. Kervella *et al.*, *A&A*, **426**, 297, 2004.
(39) A. Bressan *et al.*, *MNRAS*, **427**, 127, 2012.

The Editors congratulate David E. Holmgren (first author of the following article) on having an asteroid named after him this year: (587299) Holmgren = 2005 WJ_{209} (see the IAU WGSBN (Working Group on Small Bodies Nomenclature) Bulletin **6**, #2, 2026 February 2, p. 12).

LONG-TERM STUDIES OF EARLY-TYPE BINARY STARS: THE SPECTROSCOPIC ORBIT OF NY CEPHEI

By D. E. Holmgren[1] & S. Yang[2]

[1]*Calgary, Canada,* david.e.holmgren@gmail.com
[2]*Victoria, Canada,* syang@uvic.ca

A new spectroscopic orbit and set of absolute dimensions are presented for the early-type eclipsing binary system NY Cephei. Those results are based on 30 years of CCD spectral data obtained at the Dominion Astrophysical Observatory (DAO). A search for apsidal motion was also attempted by combining those data with older Reticon data to extend the time-base to 40 years. We present a tentative detection of apsidal motion with a period of 13 500 yr.

Introduction

NY Cephei (HD 217312, BD+62 2147) is an eclipsing binary system with components of spectral types B0·5V and B2V, in an eccentric orbit having a period of ≈ 15·3 d. It is well known for showing only one eclipse due to the combined effects of the orbital inclination and eccentricity. It has been studied previously by Tkachenko *et al.*[1], Albrecht *et al.*[2], Ahn[3], Holmgren *et al.*[4], and Heard & Fernie[5]. Moffatt[6] also proposed the system as a test of non-symmetric gravity theory, predicting a regression of the line of apsides. The search for apsidal motion is taken up further in this paper, building upon the work of Holmgren *et al.*[4]

After presenting the new CCD spectra in the next section, the measurement of radial velocities for the component stars is discussed. An initial spectroscopic orbit based on those measurements is presented. That is followed by a presentation of the component line profiles and spectroscopic orbit recovered from spectrum disentangling. Following that, the absolute dimensions and search for apsidal motion are discussed. The search for apsidal motion presented here is unique in that digital spectra covering a time interval of over 40 years are used. Finally, estimates of the projected rotational velocities are presented, based on the disentangled helium-line profiles.

Observations and reductions

The spectra presented here were obtained with the 1·2-m telescope and *McKellar* spectrograph of the Dominion Astrophysical Observatory between 1996 and 2025. The 32121H configuration of the spectrograph was used (32-inch-focal-length camera, 1200 line/mm grating, first-order diffraction, central wavelength of 660·0 nm), with the UBC-1, SITe-4, and Fletcher CCD detectors. The reciprocal dispersion was 1 nm/mm at Hα. Fig. 1 shows a typical CCD spectrum of NY Cephei. The older Reticon spectra used here in the search for apsidal motion (p. 162) were obtained with the same telescope and the 3261 configuration of the *McKellar* spectrograph (32-inch camera, 600 line/mm grating, first order, central wavelength of 420·0 nm). Those data are described in more detail by Holmgren *et al.*[4] The detectors used, and the number of spectra obtained with each, are summarized in Table I.

The red spectral region used to obtain the new spectra was chosen as that takes advantage of the higher quantum efficiency of the CCD detectors in that region. Also, for a given radial velocity the step in wavelength is larger than at shorter wavelengths. Further, the presence of telluric lines in the Hα region can help to stabilize disentangling solutions using that line.

The CCD spectra of NY Cep presented here were obtained as part of a much larger programme of monitoring early-type binary systems for Hα emission and non-radial pulsation. There are stellar lines in the 630·0–690·0 nm region that are quite suitable for radial-velocity measurement and spectral-type estimation. Specifically, lines of neutral helium, singly-ionized oxygen, and singly-ionized carbon are present.

TABLE I

Detectors used in this work.

Detector	*Number of pixels*	*Pixel size (μm)*	*Wavelength region (nm)*	*Number of spectra*
Reticon	1872	15	397·0–451·0	25
UBC-1	4096	15	630·0–690·0	8
SITe-4	4096	15	630·0–690·0	88
Fletcher	4604	13·5	630·0–690·0	2

All reductions of the CCD data were done using the IRAF processing system[7,8]. Continuum rectification of the spectra was done using a program written in GNU DATA LANGUAGE (GDL

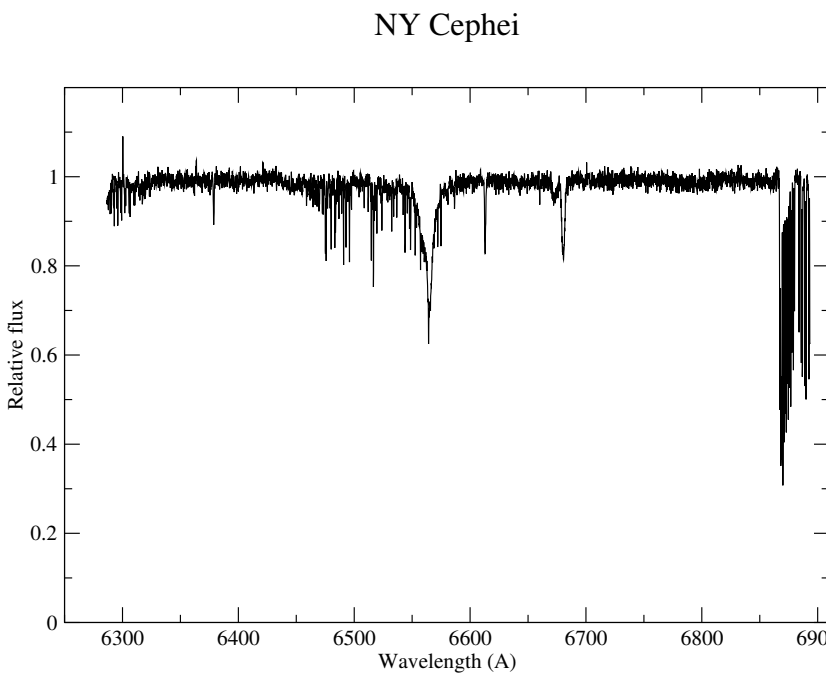

FIG. 1

A wavelength-calibrated and rectified spectrum of NY Cephei at the orbital phase corresponding to maximum radial-velocity separation.

— *e.g.*, Coulais *et al.*[9]). Heliocentric-radial-velocity corrections were done using GDL and routines from the IDL Astro library[10].

Stellar-spectrum exposures were interspersed with those of a thorium–argon arc for the wavelength calibrations. Flat-field and bias frames were also obtained on each night.

Radial-velocity measurement

Cross-correlation-function (CCF) radial-velocity measurements were done using the He I 667·8-nm region (666·5 nm–669·0 nm) and a synthetic Gaussian template with $\sigma = 25$ km/s. Using a synthetic template had the added benefit of reducing the noise in the line profiles. A typical CCF is shown in Fig. 2. The cross-correlation methodology used here follows that described by Tonry & Davis[11].

To obtain an estimate of the precision of those radial velocities, wavelength measurements of an atmospheric O_2 line (Fig. 3) on several spectra were made, and then compared to the rest wavelength from the *HITRAN* database[12]. The corresponding radial-velocity offsets are shown in Fig. 4. The standard deviation in those offset measurements is about ±1 km/s; that is an estimate of the internal error in those CCF radial velocities.

Spectroscopic orbit

A subset of the spectra was used to compute an initial spectroscopic orbit, which allowed a mass ratio to be defined. That mass ratio was then used as a constraint in the disentangling solutions, described in the next section. Only 35 spectra on which both components were

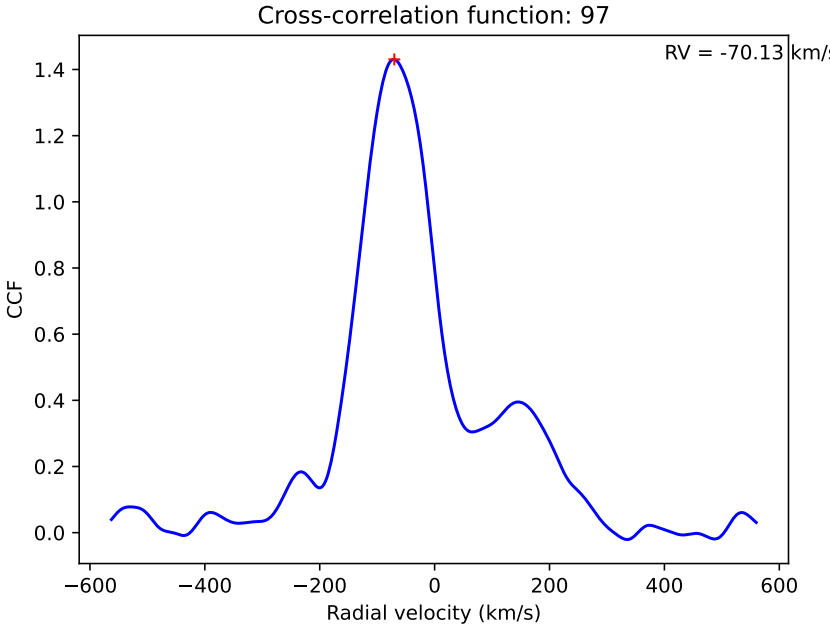

FIG. 2
An NY Cep cross-correlation function near the maximum radial-velocity separation.

visible and relatively unblended were used. A least-squares orbital solution using those data is shown in Table II. The orbital period was included in the solution as a check on previously published values. The computed value found here agrees with those presented by Ahn[3] and Albrecht *et al.*[2]

A plot of the data and fit is shown in Fig. 5. We therefore have an estimated mass ratio (P/S) of $q = 1{\cdot}282 \pm 0{\cdot}017$.

TABLE II

Spectroscopic orbit solution.

Parameter	*Value*
V_{01} (km/s)	$-14{\cdot}0 \pm 1{\cdot}2$
V_{02} (km/s)	$-7{\cdot}63 \pm 1{\cdot}50$
K_1 (km/s)	$113{\cdot}5 \pm 1{\cdot}1$
K_2 (km/s)	$145{\cdot}6 \pm 1{\cdot}4$
$q = K_2/K_1$	$1{\cdot}282 \pm 0{\cdot}017$
e	$0{\cdot}435 \pm 0{\cdot}008$
ω_0 (deg)	$53{\cdot}8 \pm 1{\cdot}8$
$T_{\rm peri} - 2400000$ (HJD)	$55116{\cdot}613 \pm 0{\cdot}056$
P (d)	$15{\cdot}27578 \pm 0{\cdot}00012$
$\sigma_{1,\rm p}$ (km/s)	$\pm 4{\cdot}10$
$\sigma_{1,\rm s}$ (km/s)	$\pm 7{\cdot}83$

The minimum masses and projected semi-major axes based on that orbit are:

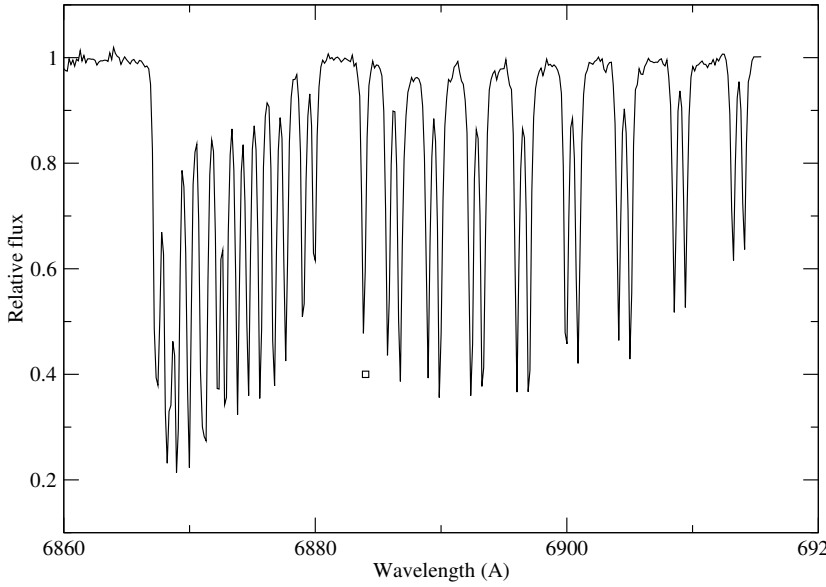

FIG. 3

A wavelength-calibrated and rectified spectrum of NY Cephei showing the O_2 line used (indicated by the square) for radial-velocity offset measurement.

$$M_1 \sin^3 i = 11{\cdot}3 \pm 0{\cdot}3\, M_\odot$$
$$M_2 \sin^3 i = 8{\cdot}8 \pm 0{\cdot}3\, M_\odot$$
$$a_1 \sin i = 30{\cdot}9 \pm 0{\cdot}4\, R_\odot$$
$$a_2 \sin i = 39{\cdot}6 \pm 0{\cdot}5\, R_\odot$$

Disentangling

Spectrum disentangling in the frequency domain[13] was used to recover the line profiles and spectroscopic orbital elements for the primary and secondary of NY Cep. That technique was implemented in the PYTHON programming language, and a more detailed description will be the subject of a forthcoming paper. A two-component version was used with the He I 667·8-nm-line data, and a three-component version with the Hα data, since it was necessary to separate out the telluric-line contribution. As spectrum disentangling does not address the Rossiter–McLaughlin (rotation) effect, spectra near the eclipse were given zero weight in the solution for the orbital parameters and line profiles. Flux factors $s_{1,2}$ were computed at all phases to account for brightness variations as a function of orbital phase. The flux factors are regarded as a fundamental quantity, since calculation of their ratio $z = s_1/s_2$ can result in the magnification of small errors, rendering that ratio of limited use. Hadrava[14] describes the flux factors in detail, and their relative values ensure that the observed line profile at any phase is reconstructed correctly. Prior to computing the disentangling solutions, all line-profile data were linearized using cubic-spline interpolation onto a radial-velocity scale with a constant sampling interval.

Each disentangling iteration involves a nonlinear simplex minimization over the orbital elements, including a linear least-squares solution for the Fourier components of the line profiles. That is followed by a linear least-squares solution for the flux factors, and the whole procedure is iterated until convergence. The disentangling-solution parameters used

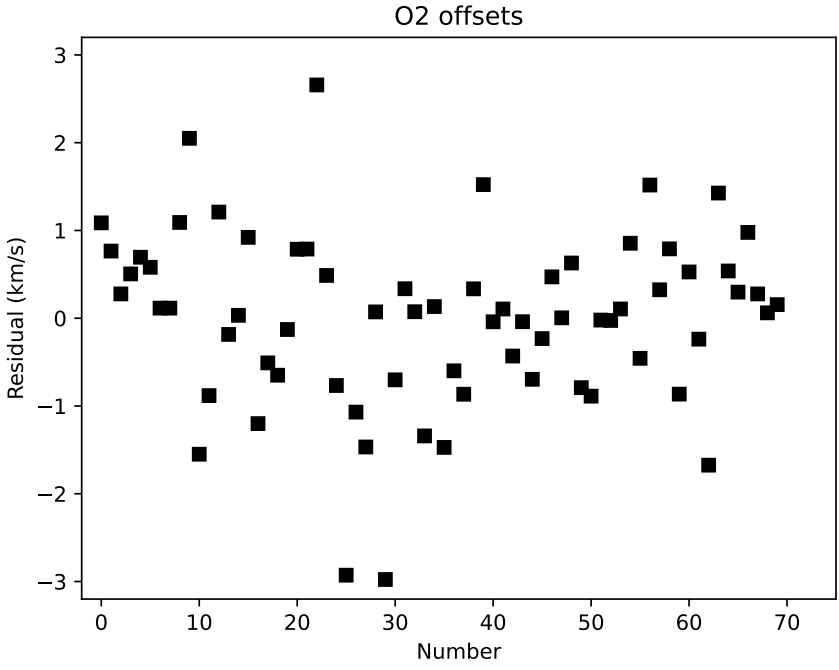

FIG. 4
The measured radial-velocity offsets in the O_2 telluric line.

in this paper are summarized in Table III. The telluric parameters were used only in the Hα solution. The function being minimized is the sum of squared residuals between the

TABLE III

Disentangling-solution parameters.

Parameter	*Unit*	*Meaning*
K_1	km/s	Primary radial-velocity semi-amplitude
K_2	km/s	Secondary radial-velocity semi-amplitude
$q = K_2/K_1$		Mass ratio (P/S)
e		Orbital eccentricity
ω_0	deg	Longitude of periastron
$\dot{\omega}$	deg/d	Apsidal-motion rate
$T_{\rm peri}$	HJD	Time of periastron passage
K_3	km/s	Telluric radial-velocity semi-amplitude
e_3		Telluric orbital eccentricity
ω_3	deg	Telluric longitude of periastron
$T_{\rm max,3}$	HJD	Time of maximum positive velocity (telluric orbit)

observed and computed line-profile Fourier components. That sum of squares is scaled to be a reduced chi-squared, so that its value is $\approx 1{\cdot}0$. The nonlinear minimization allows for the orbital parameters to be fixed or varied over a specified range. For the three-component Hα solution, the heliocentric-radial-velocity corrections $V_\odot$ are used as a constraint on the

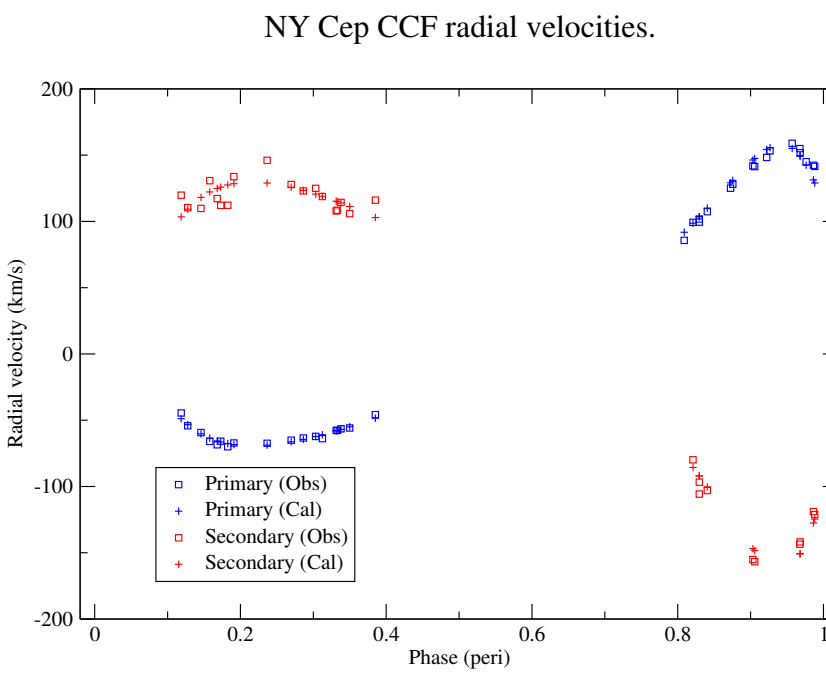

FIG. 5
The measured CCF radial velocities (squares) and computed orbit (plus signs).

telluric parameters. That part of the fit is indicative of the solution quality for K_3, $T_{\max,3}$ and ω_3. Also, $T_{\max,3}$ is used due to the small eccentricity of the Earth's orbit, following Sterne's recommendation[15,16].

At the end of each disentangling iteration, the computed flux factors $s_{1,2}$ are used in a minimization to recover a value of the light ratio[14]. The uncertainty in the light ratio may be computed by measuring the noise levels in the recovered profiles and then using error propagation.

After converging a disentangling solution, radial velocities were measured from the line-profile data by sliding and scaling the recovered component line profiles to fit the observed profiles. The computed flux factors were used for the scaling. Also, the mass ratio was used as a constraint on the measured radial velocities.

The He I 667·8-nm line-profile data set is shown in Fig. 6. Certain very noisy profiles were given zero weight in the disentangling solution. For that solution, the radial-velocity sampling interval was 2·5 km/s. Weights were assigned to each profile according to its signal-to-noise ratio.

The orbital period was fixed at $P = 15{\cdot}27566$ d, following Ahn[3] and Albrecht *et al.*[2] That same value of the period was also used in the Hα solution.

The final orbital parameters derived from He I 667·8 nm are shown in Table IV. Errors in the orbital parameters were computed by examining the variation in the sum of squares of residuals as a function of each parameter independently. A parabolic fit to the minimum then gave an estimate of the parameter error. Note that that method does not account for inter-parameter correlations. That approach to error calculation was found to be more effective than inverting the Hessian matrix at the solution point.

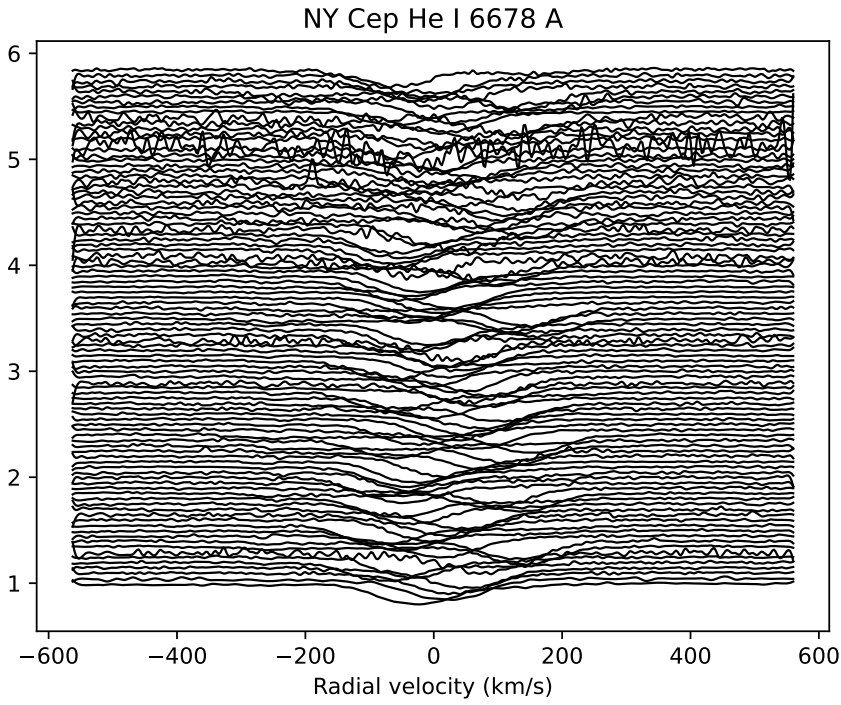

FIG. 6

The line-profile data for He I 667·8 nm in NY Cep. The spectra are ordered with the earliest at the bottom and the most recent at the top of the plot.

The final component line profiles are shown in Fig. 7, the measured and computed radial velocities in Fig. 8, and the flux factors in Fig. 9. The r.m.s. errors for the measured radial velocities were ±1·24 km/s and ±1·80 km/s for the primary and secondary, respectively.

The measured flux factors were used to recover the light ratio, indicating $l(\mathrm{P/S}) = 4{\cdot}08 \pm 0{\cdot}10$.

TABLE IV

Orbital elements from He I 667·8 nm.

Parameter	*Value*
K_1 (km/s)	113·9 ± 0·5
q	1·241 ± 0·069
K_2 (km/s)	141·4 ± 0·5
e	0·4391 ± 0·0008
ω_0 (deg)	57·5 ± 1·1
$T_{\mathrm{peri}} - 240000$ (HJD)	55116·751 ± 0·067

The flux factors indicate quite clearly the presence of the primary eclipse near phase 0·63. Also, near phase 0·05, there is a hint of a secondary eclipse. However, that could also be interpreted as the rotation (Rossiter–McLaughlin) effect.

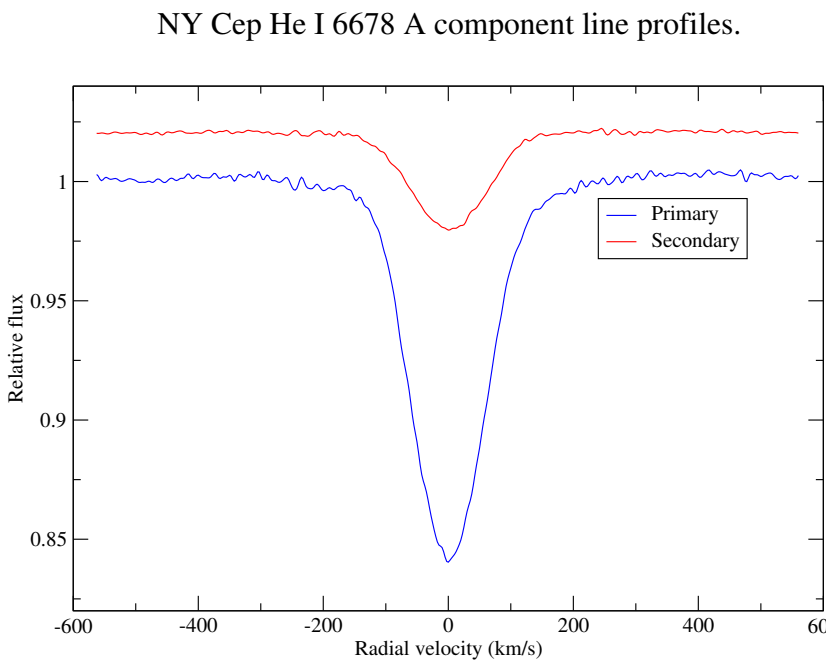

FIG. 7

The primary (bottom) and secondary (top) line profiles for He I 667·8 nm in NY Cep. The secondary profile has been displaced upward for clarity.

The solution for the Hα-profile data is shown in Table V and Fig. 10, Fig. 11, & Fig. 12. That solution converged in 80 iterations. The line-profile data used in that solution are shown in Fig. 13. Once again, weights proportional to the signal-to-noise for each spectrum were used. The r.m.s. errors of the radial velocities measured from the Hα profiles were ±0·73 km/s for the primary and ±0·90 km/s for the secondary.

A radial-velocity sampling interval of 6 km/s was used for the Hα solution. The eccentricity and period for the telluric orbit were held fixed at 0·0167301 and 365·2422 d, respectively. Once again, the flux factors show the presence of the primary eclipse and possible secondary eclipse or rotation effect. However, the noise level in those is much greater than that in the solution of the He I 667·8-nm data set.

The heliocentric velocity corrections $V_\odot$ were used to constrain the telluric parameters. That part of the fit is shown in Fig. 14.

Due to the high declination of NY Cep, the telluric radial velocities cover a range of only about ±15 km/s, which is slightly larger than two radial-velocity sampling bins. That and unavoidable small rectification errors limited the solution quality for the telluric line profile. To some extent, it is possible to fix that using band-pass filtering once the Fourier components of the line profiles have converged.

The telluric line profile shows the rotational lines of the H_2O molecule.

The light ratio (P/S) measured from the depths of the recovered primary and secondary line profiles is $l = 3{\cdot}74 \pm 0{\cdot}10$.

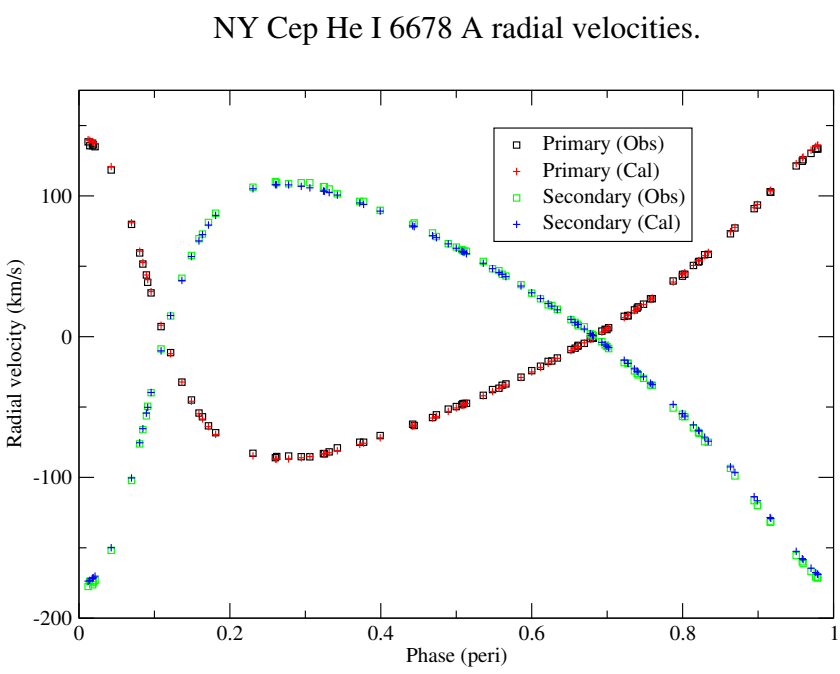

FIG. 8
The measured and computed radial velocities for He I 667·8 nm in NY Cep.

TABLE V

Orbital elements from Hα.

Parameter	*Value*
K_1 (km/s)	106·4 ± 4·6
$q = K_2/K_1$	1·33 ± 0·10
K_2 (km/s)	141·9 ± 12·8
e	0·430 ± 0·024
ω_0 (deg)	51·8 ± 3·1
$T_{\rm peri}$ − 240000 (HJD)	55116·725 ± 0·059
K_3 (km/s)	14·89
ω_3 (deg)	166·74
$T_{\rm max,3}$ − 240000 (HJD)	55034·5

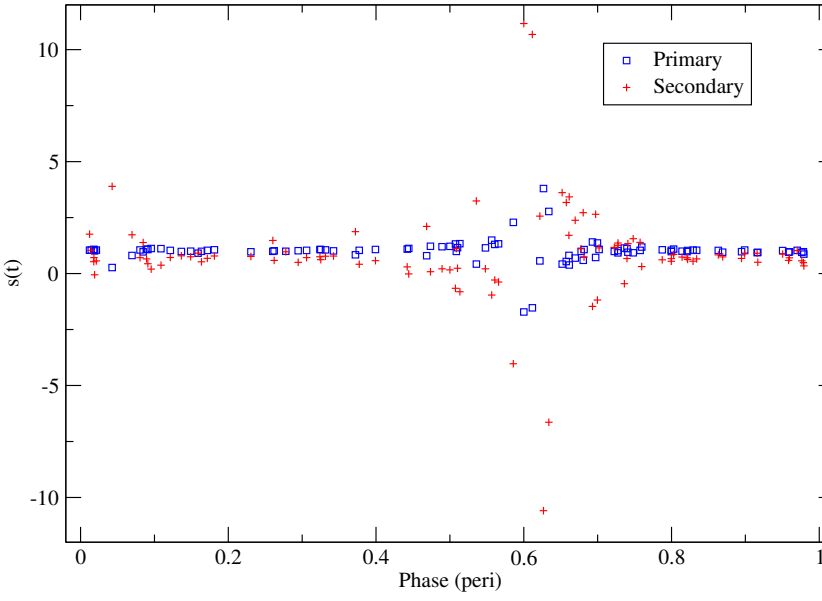

FIG. 9

Flux factors for He I 667·8 nm in NY Cep. Squares denote the primary, plus signs the secondary.

Search for apsidal motion

A search for apsidal motion was done by computing a disentangling solution which combined the new He I 667·8-nm data with the older He I 447·1-nm–Mg II 448·1-nm Reticon data from Holmgren *et al.*[4] As with the other disentangling solutions, the Reticon data were given weights proportional to the signal-to-noise of each spectrum. Also, since the Reticon data were obtained at a resolution approximately half of that of the CCD data, they were given half the weight in the disentangling solution for the combined data set.

The computed solution is shown in Table VI. Note that the apsidal-motion rate $\dot{\omega}$ is included, and that it has a large uncertainty due to the relatively short time interval used to estimate it.

TABLE VI

Orbital elements from the combined solution.

Parameter	*Value*
K_1 (km/s)	111·70 ± 0·1
$q = K_2/K_1$	1·29 ± 0·02
K_2 (km/s)	144·1 ± 0·1
e	0·4435 ± 0·0006
ω_0 (deg)	60·9 ± 0·2
$T_{\rm peri} - 240000$ (HJD)	55116·853 ± 0·049
$\dot{\omega}$ (rad/d)	$1{\cdot}28 \times 10^{-6}$
U (yr)	13500

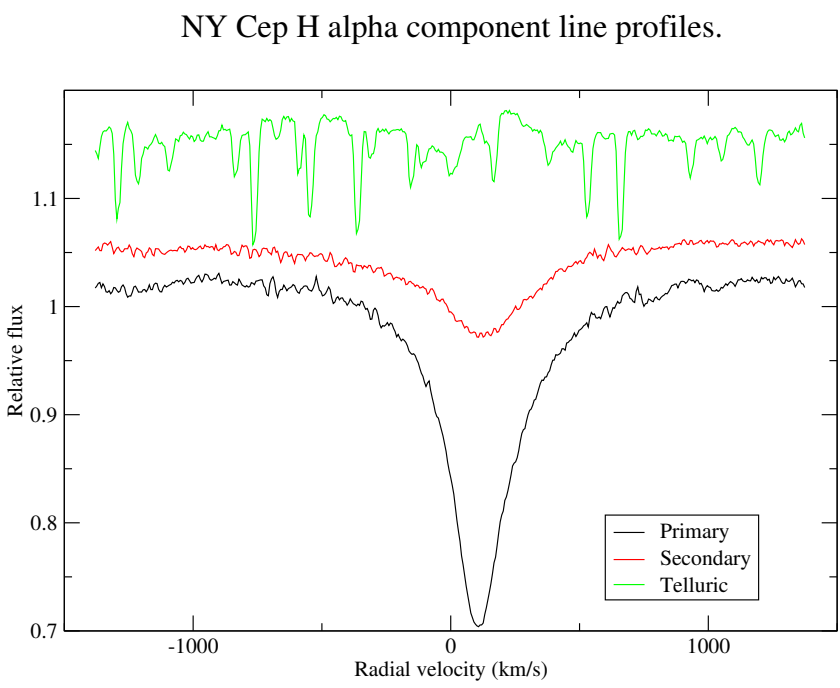

FIG. 10

The primary (bottom) and secondary (middle) and telluric (top) line profiles for Hα in NY Cep. The secondary and telluric profiles have been displaced upward for clarity.

The theoretical apsidal-motion period [16,17], including both classical and relativistic contributions, is 4445 yr. That is discussed in more detail in the section on absolute dimensions. The difference between the observed and theoretical rates is not unexpected given the relatively short time-base used to estimate the former. Future observations should allow that observed apsidal period to be refined.

The recovered He I 667·8-nm profiles are shown in Fig. 15, and the flux factors in Fig. 16. The profiles show good agreement with those obtained from the solution of the CCD data alone.

The recovered He I 447·1-nm and Mg II 448·1-nm profiles are shown in Fig. 17, and the flux factors for that region in Fig. 18. The flux factors for that region indicate the presence of the primary eclipse, and a possible secondary eclipse or rotation effect. We note the good inter-agreement between the two sets of flux factors.

The computed light ratio (P/S) for the He I 667·8-nm region was 4·43 ± 0·07 and that for the He I 447·1-nm–Mg II 448·1-nm region was 2·38 ± 0·07. The former light ratio shows good agreement with that found from the measured equivalent widths.

Spectrophotometry

The disentangled He I 667·8-nm line profiles from the combined solution were measured for equivalent width. Integration of the profiles gave EW_p = 0·0549 nm and EW_s = 0·0115 nm. Those then give a light ratio (P/S) of l = 4·76.

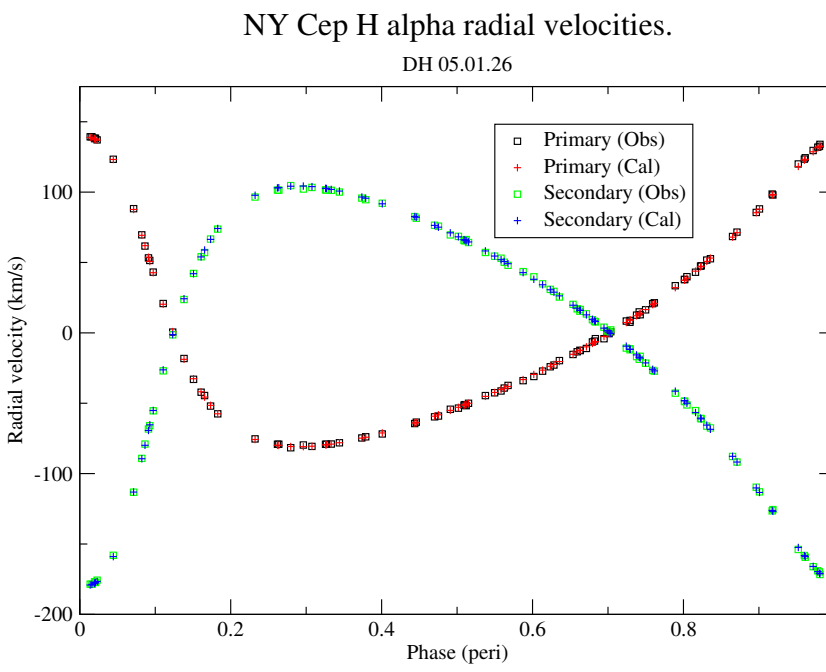

FIG. 11
The measured and computed radial velocities for Hα in NY Cep.

Synthetic spectra from the *POLLUX* database[18] were used to estimate the projected rotational velocities of the components. Using the He I 667·8-nm line, a NLTE model with $T_{\rm eff}$ = 28 000 K and log g = 4·0, when convolved with a rotational line profile having $v \sin i$ = 80 km/s, produced a satisfactory fit for the primary. Similarly, a model with $T_{\rm eff}$ = 23 000 K, log g = 4·0, and $v \sin i$ = 100 km/s gave a satisfactory fit for the secondary. Those fits also include a Gaussian instrumental profile having a FWHM of 12 km/s, estimated from the widths of relatively unblended telluric O_2 lines. No attempt was made to fit those profiles in a least-squares sense due to the coarse nature of the model-atmosphere grid. Prior to the fitting, each profile was corrected according to the light ratio. Those results for the projected rotational velocities are in agreement with those from Holmgren *et al.*[4] and Albrecht *et al.*[2]

Absolute dimensions

The minimum masses and projected semi-major axes computed using the different orbital solutions are compared in Table VII. Note that the last line in that table refers to the combined solution used to search for apsidal motion.

The minimum masses and projected semi-major axes from the different solutions are in good agreement. However, the errors for the Hα line are larger than those for the other solutions. In particular, the disentangling solution for the combined data sets and the orbit based on the CCF radial velocities are in excellent agreement. We therefore adopt the results from the combined disentangling solution, which are in good agreement with those from Albrecht *et al.*[2]

Using the minimum masses, projected semi-major axes, and the mean fractional radii from

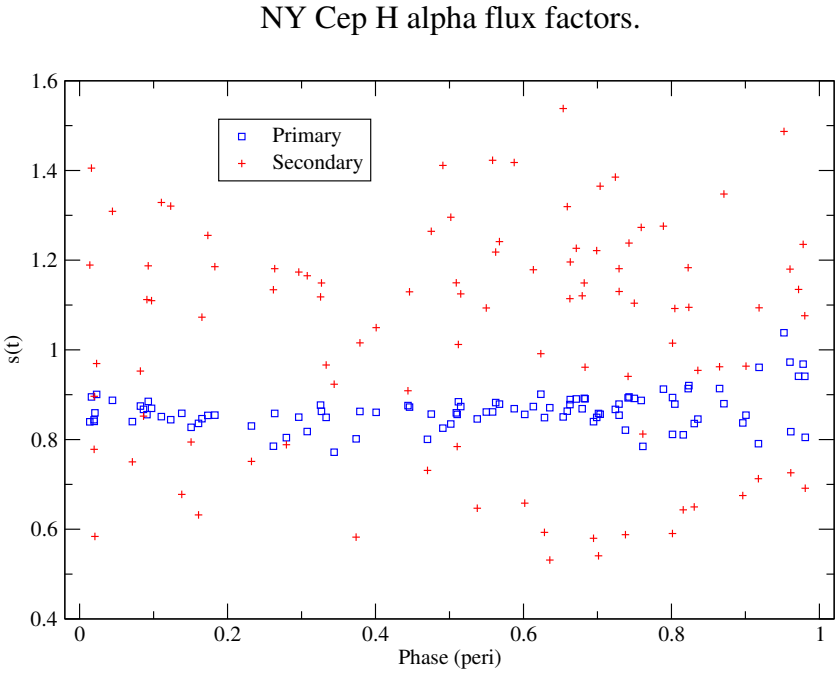

FIG. 12

Flux factors for Hα in NY Cep. Squares denote the primary, plus signs the secondary.

TABLE VII

Comparison of minimum masses and projected semi-major axes.

Method	$M_1 \sin^3 i\ (M_\odot)$	$M_2 \sin^3 i\ (M_\odot)$	$a_1 \sin i\ (R_\odot)$	$a_2 \sin i\ (R_\odot)$
CCF	11·3 ± 0·3	8·8 ± 0·3	30·9 ± 0·4	39·6 ± 0·5
He I 6678	10·6 ± 0·7	8·5 ± 0·7	30·9 ± 0·1	38·4 ± 2·1
Hα	10·2 ± 1·4	7·6 ± 1·2	29·0 ± 1·5	38·7 ± 3·6
Combined soln.	11·7 ± 0·3	8·7 ± 0·2	30·23 ± 0·03	40·5 ± 0·8

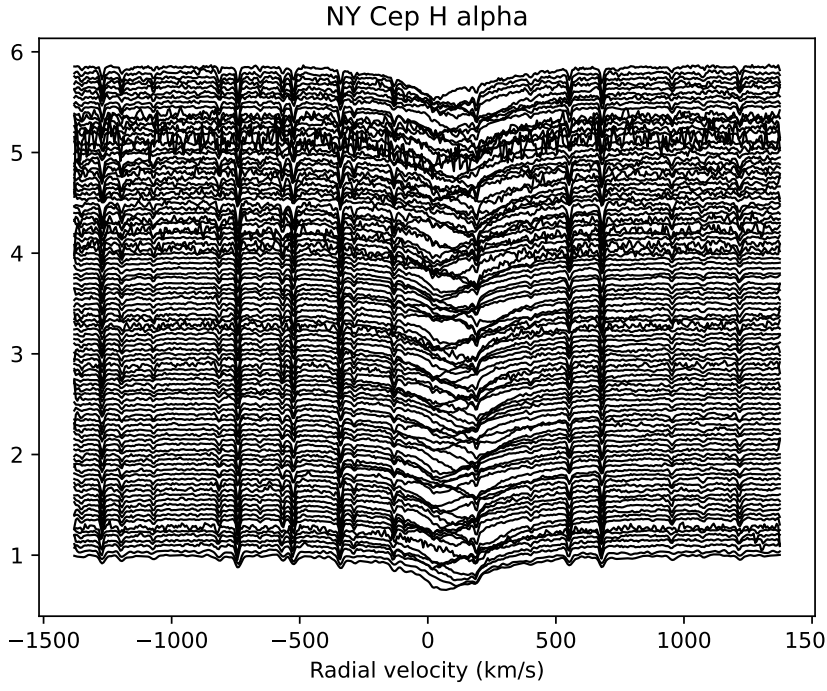

FIG. 13

The Hα-line-profile data for NY Cep. The spectra are ordered with the earliest at the bottom and the most recent at the top of the plot.

Ahn[3], we find the following absolute masses and radii:

$$\begin{aligned} M_1 &= 12{\cdot}1 \pm 0{\cdot}3\, M_\odot \\ M_2 &= 9{\cdot}4 \pm 0{\cdot}3\, M_\odot \\ R_1 &= 6{\cdot}8 \pm 0{\cdot}5\, R_\odot \\ R_2 &= 5{\cdot}7 \pm 0{\cdot}5\, R_\odot \end{aligned}$$

Those are quite similar to the results found by Holmgren *et al.*[4] and slightly larger than those from Albrecht *et al.*[2]

From the estimated projected rotational velocities, orbital period, and inclination, we find that the primary and secondary components rotate faster than the Keplerian rate at periastron by factors of 3·6 and 5·4 respectively.

Using the absolute dimensions, the orbital eccentricity from the combined disentangling solution, and internal structure constants $\log_{10} k_2$ from Claret[19], a theoretical apsidal period of 4445 yr is found. From Claret's[19] tables, for the primary $\log_{10} k_2 = -2{\cdot}193$ and for the secondary $\log_{10} k_2 = -2{\cdot}234$. The corresponding system age is $\approx 10^7$ yr.

The classical and relativistic contributions to P/U are[17]:

$$\begin{aligned} [P/U]_{\rm cl} &= 7{\cdot}044 \times 10^{-6} \\ [P/U]_{\rm rel} &= 2{\cdot}364 \times 10^{-6} \end{aligned}$$

Those show that the relativistic contribution is about a factor of three smaller than the classical part.

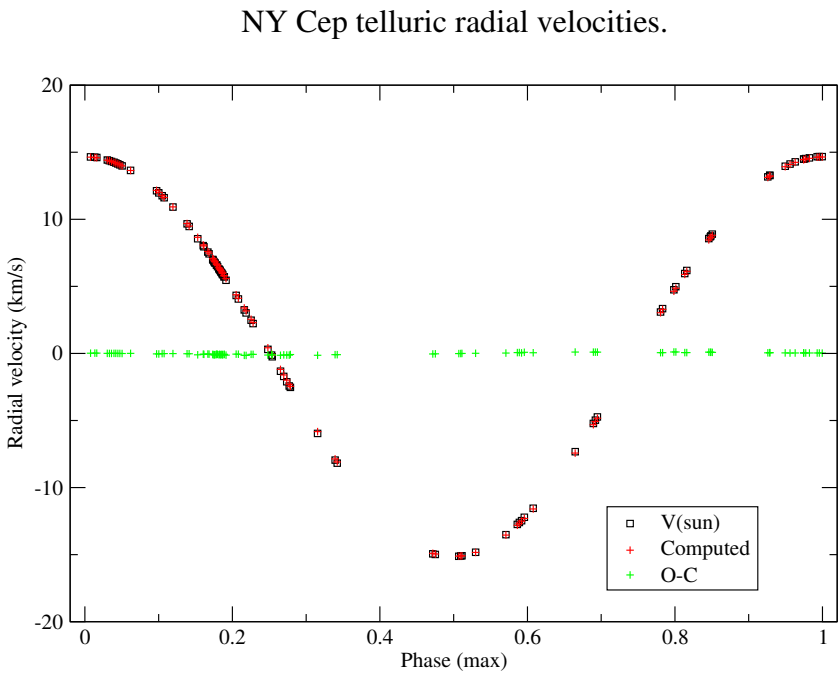

FIG. 14

Telluric-line radial velocities from the Hα solution. Squares denote $V_\odot$ values, plus signs denote computed radial velocities, and crosses denote fit residuals.

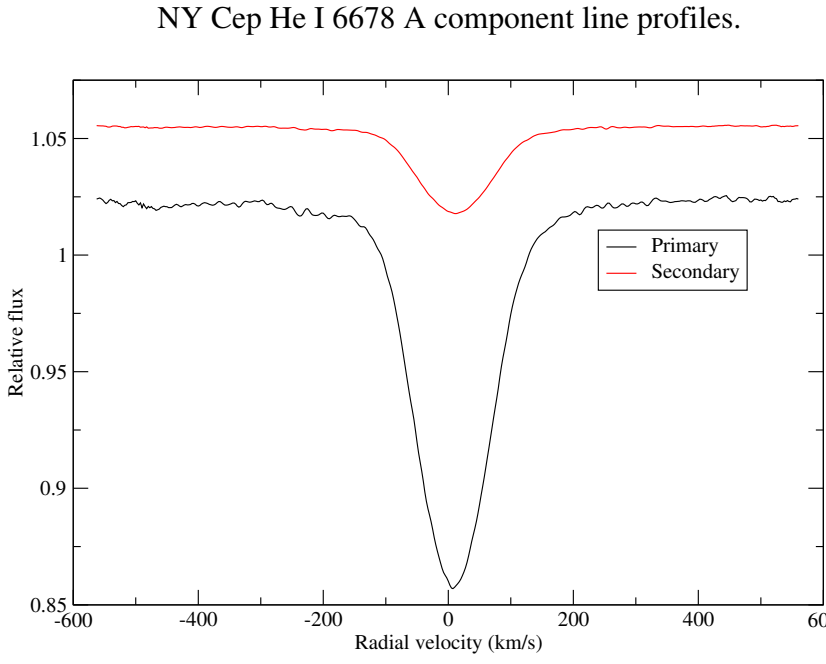

FIG. 15

The recovered He I 667·8-nm line profiles for the primary (bottom) and secondary (top) using both CCD and Reticon data.

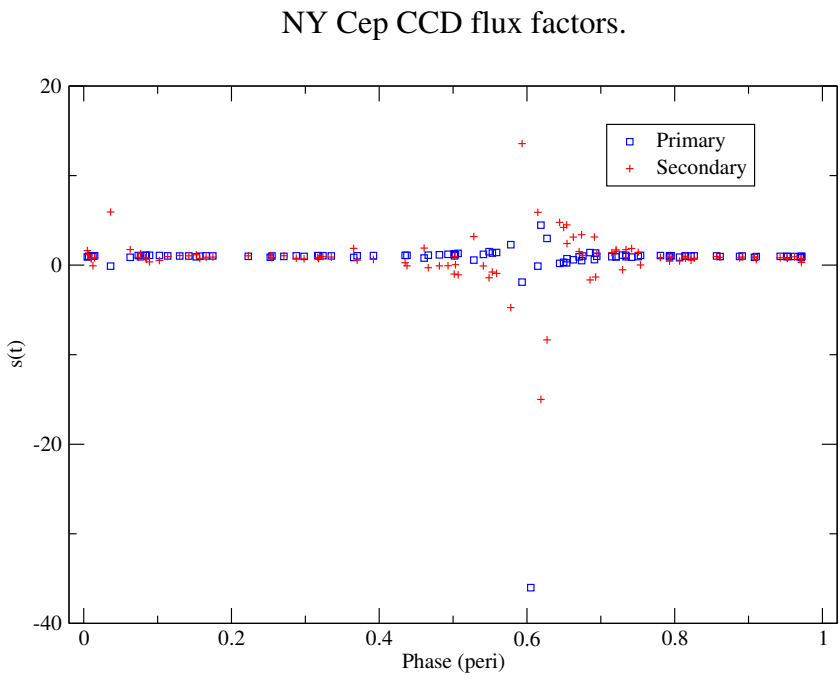

FIG. 16

The flux factors for the He I 667·8-nm region. Squares denote the primary, plus signs the secondary. Both CCD and Reticon data were used.

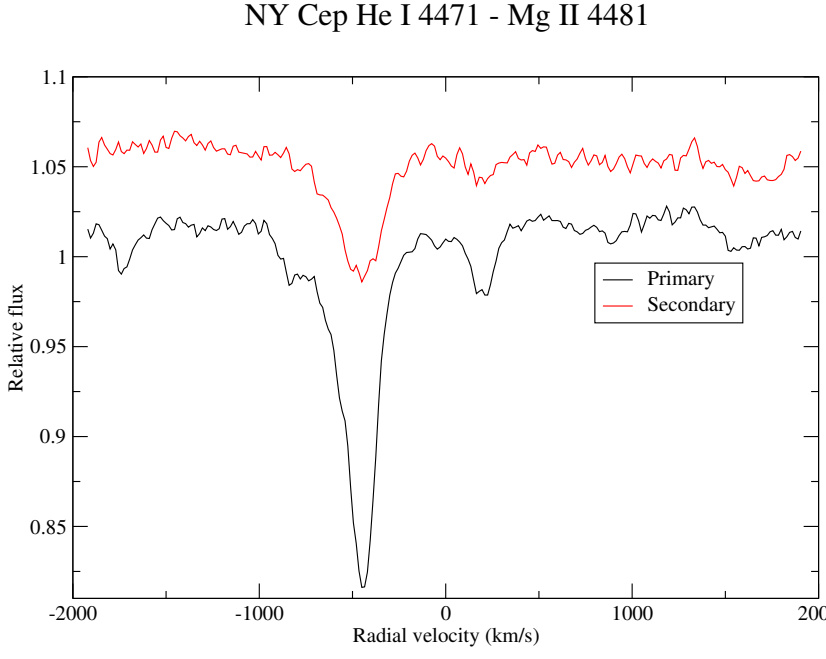

FIG. 17

The recovered He I 447.1 nm–Mg II 448.1 nm line profiles for the primary (bottom) and secondary (top) using both CCD and Reticon data.

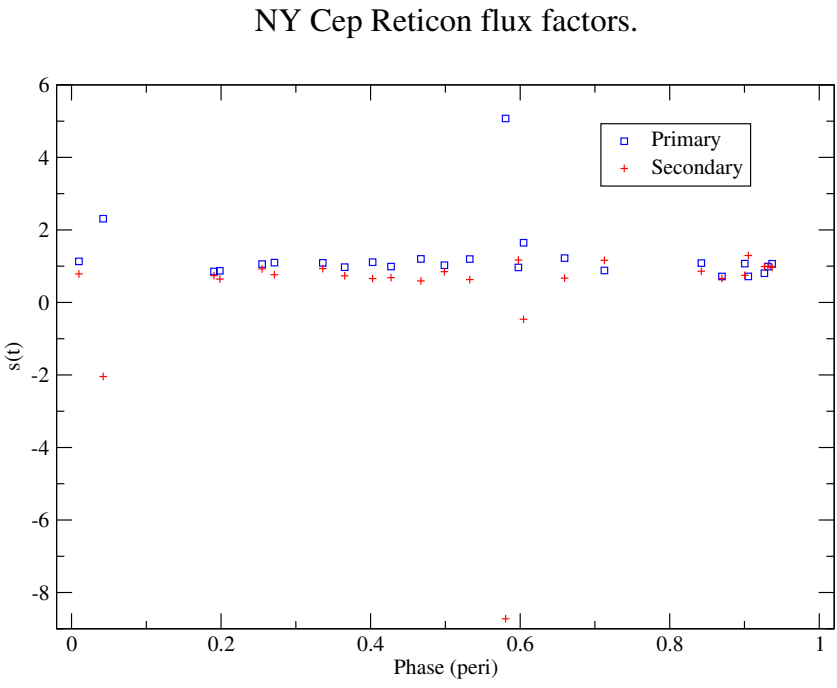

FIG. 18

The flux factors for the He I 447.1 nm–Mg II 448.1 nm region. Squares denote the primary, plus signs the secondary. Both CCD and Reticon data were used.

Radial-velocity measurements.

Table VIII

NY Cep He I 667·8-nm radial velocities.

Filename	*HJD* − 2400000·0	*Phase (peri)*	V_1(*Obs*)	(*O-C*)$_1$	V_2(*Obs*)	(*O-C*)$_2$	*Weight*
6279	51381·9671	0·5024	−47·72	−0·19	64·41	0·24	1·19
6448	51384·8660	0·6921	5·22	0·00	−7·06	−0·01	0·72
13066	51461·0044	0·6764	0·13	−0·00	−0·19	−0·02	1·34
13397	51461·8926	0·7346	19·91	0·05	−26·89	−0·07	1·21
11577	51437·9386	0·1665	−61·95	−0·13	83·57	0·10	1·44
12577	51451·9574	0·0842	47·30	0·10	−63·82	−0·10	1·40
2053	51599·6789	0·7546	27·35	0·09	−36·91	−0·10	0·31
11679	53587·9145	0·9117	99·95	0·04	−134·96	−0·05	1·60
12059	53588·8244	0·9712	128·98	0·05	−174·23	−0·14	1·53
12405	53589·8375	0·0375	118·46	0·14	−159·88	−0·11	1·30
12756	53590·8472	0·1036	12·13	0·02	−16·38	−0·04	1·69
13153	53591·9521	0·1760	−67·67	−0·09	91·36	0·11	1·18
12523	53949·8686	0·6065	−20·84	−0·09	28·13	0·12	1·16
12874	53950·9199	0·6753	−0·23	0·00	0·37	0·06	0·71
13184	53951·9536	0·7430	23·08	0·15	−31·18	−0·21	0·87
18117	54003·0192	0·0859	44·16	0·19	−59·63	−0·27	1·10
17633	54400·8789	0·1313	−28·97	−0·09	39·08	0·08	1·47
15683	54367·9168	0·9734	129·75	0·04	−175·27	−0·12	1·34
408	54490·7398	0·0139	132·87	0·00	−179·40	0·00	1·19
10250	54659·9413	0·0904	35·78	0·10	−48·28	−0·11	1·61
10647	54660·9817	0·1585	−56·21	−0·10	75·89	0·13	0·90
1129	54862·7489	0·3669	−75·36	−0·03	101·76	0·04	1·05
15558	55031·8836	0·4391	−61·68	−0·05	83·34	0·13	1·41
16241	55032·9411	0·5083	−46·23	−0·12	62·43	0·17	1·58
4627	54912·0579	0·5949	−24·13	−0·16	32·53	0·17	1·13
7683	54960·9367	0·7947	43·38	0·13	−58·54	−0·13	1·34
8369	54961·9076	0·8582	72·33	0·12	−97·63	−0·12	1·71
30517	55149·7321	0·1539	−52·49	−0·15	70·86	0·18	1·35
23719	55100·8429	0·9534	121·58	0·14	−164·11	−0·14	1·91
24272	55101·8009	0·0161	132·13	−0·01	−178·42	−0·00	1·41
24845	55102·7048	0·0753	63·55	0·11	−85·80	−0·14	1·19
3163	55248·6399	0·6288	−14·50	−0·11	19·53	0·10	1·45
3706	55249·6451	0·6946	6·01	−0·01	−8·11	0·01	1·57
996	55219·6501	0·7310	18·61	0·05	−25·13	−0·06	0·98
1505	55220·6215	0·7946	43·28	0·06	−58·48	−0·13	1·09
19605	55499·7061	0·0645	82·43	0·06	−111·33	−0·09	1·43
19988	55500·9190	0·1439	−43·11	−0·08	58·24	0·13	1·11
17148	55464·8449	0·7823	38·29	0·13	−51·67	−0·15	1·54
10032	55769·9002	0·7523	26·54	0·12	−35·82	−0·14	0·51
10405	55770·8698	0·8158	52·49	0·12	−70·90	−0·19	1·28
7914	55738·8907	0·7223	15·52	0·02	−20·91	0·02	1·15
16449	55857·7535	0·5035	−47·35	−0·10	63·89	0·10	1·16
15135	55823·9310	0·2894	−85·04	−0·04	114·88	0·11	1·04
13715	56165·7258	0·6645	−3·66	−0·04	4·92	0·03	1·81
14231	56166·8150	0·7358	20·38	0·07	−27·53	−0·10	1·14
6795	56073·9411	0·6560	−6·27	−0·00	8·45	−0·01	0·77
7362	56074·9567	0·7224	15·58	0·05	−21·02	−0·05	0·43
20927	56220·8426	0·2727	−85·87	−0·06	115·97	0·10	0·87
17601	56193·6859	0·4949	−49·37	−0·10	66·65	0·12	0·80
18066	56194·6909	0·5607	−33·15	−0·06	44·81	0·13	1·60

(continued on next page)

Filename	*HJD − 2400000·0*	*Phase (peri)*	V_1*(Obs)*	$(O\text{-}C)_1$	V_2*(Obs)*	$(O\text{-}C)_2$	*Weight*
3772	56384·0150	0·9545	122·03	0·09	−164·79	−0·13	1·31
2614	56382·0216	0·8240	56·13	0·09	−75·76	−0·09	1·01
3161	56383·0241	0·8897	88·30	0·07	−119·23	−0·10	1·17
14880	56558·7609	0·3940	−70·67	−0·12	95·47	0·20	1·09
11893	56927·6512	0·5429	−37·73	−0·10	50·94	0·13	1·59
12307	56928·7774	0·6166	−17·91	−0·03	24·18	0·04	1·19
12812	56929·6309	0·6725	−1·12	−0·00	1·59	0·09	1·60
11819	57291·6573	0·3721	−74·35	0·12	100·26	−0·29	1·26
12455	57292·6497	0·4370	−62·26	−0·20	83·91	0·11	1·55
13032	57293·6905	0·5052	−46·99	−0·13	63·44	0·17	1·42
10972	57649·7896	0·8167	52·87	0·11	−71·39	−0·15	0·98
8673	57942·9329	0·0069	134·37	0·01	−181·43	−0·01	0·33
9658	57949·9838	0·4685	−55·39	−0·11	74·75	0·11	0·32
4545	57900·9241	0·2569	−86·00	−0·07	116·16	0·13	0·97
5286	57901·8892	0·3201	−82·12	−0·02	110·91	0·05	0·85
19234	58054·9081	0·3372	−79·97	−0·08	108·00	0·13	0·60
9926	58390·6919	0·3189	−82·28	−0·04	111·13	0·08	0·90
10667	58747·8054	0·6968	6·75	−0·02	−9·12	0·02	0·39
10070	59478·8799	0·5556	−34·51	−0·11	46·60	0·14	0·86
8164	59820·8982	0·9453	117·68	0·14	−158·86	−0·16	0·60
8277	59821·8736	0·0092	134·01	0·02	−180·86	0·06	0·54
1335	59633·6570	0·6878	3·79	−0·02	−5·11	0·04	0·59
92	59589·6828	0·8091	49·54	0·11	−66·88	−0·13	0·35
11230	59864·9467	0·8289	58·38	0·11	−78·85	−0·17	0·58
11359	59865·9399	0·8939	90·53	0·05	−122·28	−0·11	0·64
9581	59847·9677	0·7174	13·86	0·09	−18·70	−0·10	0·50
867	60004·6447	0·9740	130·07	0·15	−175·60	−0·17	0·37
5781	60131·8417	0·3008	−84·12	−0·02	113·67	0·11	0·55
5061	60120·8407	0·5807	−27·94	−0·12	37·68	0·11	0·70
5152	60121·8515	0·6468	−8·93	0·11	12·06	−0·15	0·52
11220	60249·6464	0·0127	133·27	0·08	−179·95	−0·11	0·74
11768	60271·8057	0·4634	−56·55	−0·13	76·29	0·12	0·52
11911	60272·8336	0·5307	−40·78	−0·09	55·05	0·11	0·56
10206	60222·7974	0·2551	−86·03	−0·13	116·15	0·17	0·07
10326	60223·8865	0·3264	−81·45	−0·12	109·93	0·12	0·48
1238	60432·9564	0·0129	133·16	0·01	−179·88	−0·10	0·33
1356	60433·9744	0·0795	55·89	0·12	−75·45	−0·15	0·43
1650	60444·9462	0·7978	44·70	0·13	−60·33	−0·16	0·40
1733	60445·9598	0·8641	75·17	0·03	−101·50	−0·04	0·33
3201	60503·8891	0·6564	−6·12	0·02	8·26	−0·02	1·34
5661	60556·7413	0·1163	−8·13	0·17	11·00	−0·21	1·21
1480	60686·6642	0·6215	−13·62	2·86	18·27	−3·99	0·69
169	60721·6341	0·9108	99·46	0·02	−134·31	−0·04	0·74
4975	60859·9437	0·9650	126·59	0·05	−170·88	−0·02	0·75
6693	60900·9947	0·6524	−7·35	0·02	9·91	−0·03	0·74
7504	60928·9772	0·4842	−51·88	−0·14	70·04	0·18	0·77
7596	60930·0041	0·5514	−35·64	−0·17	48·08	0·18	0·80
8787	60970·8513	0·2254	−83·54	−0·03	112·88	0·12	0·70

(continued from previous page)

Table IX

NY Cep Hα radial velocities.

Filename	*HJD* − 2400000·0	*Phase (peri)*	$V_1(Obs)$	$(O\text{-}C)_1$	$V_2(Obs)$	$(O\text{-}C)_2$	*Weight*
6279	51381·9671	0·5092	−51·31	0·02	65·71	−0·50	1·19
6448	51384·8660	0·6990	0·90	2·12	1·34	−0·23	0·72
13066	51461·0044	0·6833	−4·15	2·10	7·80	−0·25	1·34
13397	51461·8926	0·7414	14·91	1·48	−18·78	−1·45	1·21
11577	51437·9386	0·1733	−51·99	−0·52	66·67	0·27	1·44
12577	51451·9574	0·0910	53·27	−0·47	−68·30	1·02	1·40
2053	51599·6789	0·7614	21·36	0·42	−27·21	−0·19	0·31
11679	53587·9145	0·9185	97·96	−0·35	−125·55	1·27	1·60
12059	53588·8244	0·9781	131·97	0·49	−169·07	0·54	1·53
12405	53589·8375	0·0444	123·34	0·12	−158·03	0·92	1·30
12756	53590·8472	0·1105	20·86	0·51	−26·99	−0·73	1·69
13153	53591·9521	0·1828	−57·52	−0·03	73·71	−0·45	1·18
12523	53949·8686	0·6133	−27·19	−0·71	34·84	0·69	1·16
12874	53950·9199	0·6821	−5·84	0·76	8·18	−0·33	0·71
13184	53951·9536	0·7498	16·38	−0·16	−21·56	−0·22	0·87
18117	54003·0192	0·0928	51·45	0·79	−65·94	−0·59	1·10
17633	54400·8789	0·1381	−18·22	0·58	23·69	−0·55	1·47
15683	54367·9168	0·9803	132·52	0·10	−169·80	1·02	1·34
408	54490·7398	0·0207	138·29	0·73	−177·31	0·14	1·19
10250	54659·9413	0·0973	43·15	0·40	−55·38	−0·23	1·61
10647	54660·9817	0·1654	−44·54	1·09	57·07	−1·80	0·90
1129	54862·7489	0·3738	−74·67	0·14	95·74	−0·77	1·05
15558	55031·8836	0·4459	−63·45	0·24	81·45	−0·72	1·41
16241	55032·9411	0·5152	−50·04	0·01	64·17	−0·40	1·58
4627	54912·0579	0·6017	−31·02	−1·48	39·78	1·68	1·13
7683	54960·9367	0·8015	37·98	0·58	−48·82	−0·58	1·34
8369	54961·9076	0·8651	68·49	0·48	−87·81	−0·09	1·71
30517	55149·7321	0·1607	−42·13	−0·29	54·07	0·09	1·35
23719	55100·8429	0·9603	123·43	0·73	−158·18	0·10	1·91
24272	55101·8009	0·0230	137·11	0·24	−175·72	0·84	1·41
24845	55102·7048	0·0822	69·64	0·31	−89·18	0·25	1·19
3163	55248·6399	0·6356	−19·72	0·66	25·44	−0·86	1·45
3706	55249·6451	0·7014	−0·54	−0·11	0·91	0·37	1·57
996	55219·6501	0·7378	12·61	0·49	−16·85	−1·20	0·98
1505	55220·6215	0·8014	37·84	0·48	−48·48	−0·29	1·09
19605	55499·7061	0·0713	88·23	0·55	−113·22	−0·10	1·43
19988	55500·9190	0·1507	−33·02	−0·42	42·23	0·18	1·11
17148	55464·8449	0·7892	33·48	1·36	−42·86	−1·42	1·54
10032	55769·9002	0·7592	20·76	0·67	−26·66	−0·75	0·51
10405	55770·8698	0·8227	47·40	0·48	−60·77	−0·24	1·28
7914	55738·8907	0·7292	7·50	−1·54	−11·23	0·43	1·15
16449	55857·7535	0·5104	−51·02	0·06	65·40	−0·49	1·16
15135	55823·9310	0·2962	−79·68	1·16	102·20	−2·07	1·04
13715	56165·7258	0·6714	−11·09	−1·17	13·48	0·68	1·81
14231	56166·8150	0·7427	12·88	−1·01	−16·66	1·25	1·14
6795	56073·9411	0·6628	−12·41	0·10	15·37	−0·77	0·77
7362	56074·9567	0·7293	8·85	−0·22	−12·06	−0·35	0·43
20927	56220·8426	0·2795	−81·61	−0·86	104·63	0·47	0·87
17601	56193·6859	0·5017	−53·48	−0·59	68·56	0·32	0·80
18066	56194·6909	0·5675	−37·35	0·76	48·01	−1·15	1·60
3772	56384·0150	0·9614	124·41	1·13	−159·40	−0·36	1·31
2614	56382·0216	0·8309	51·71	0·92	−66·28	−0·76	1·01
3161	56383·0241	0·8965	85·58	0·18	−109·65	0·51	1·17

(continued on next page)

Filename	*HJD − 2400000·0*	*Phase (peri)*	$V_1(Obs)$	$(O\text{-}C)_1$	$V_2(Obs)$	$(O\text{-}C)_2$	*Weight*
14880	56558·7609	0·4009	−71·83	−0·73	92·10	0·39	1·09
11893	56927·6512	0·5498	−42·56	−0·24	54·47	−0·11	1·59
12307	56928·7774	0·6235	−24·11	−0·37	30·90	0·28	1·19
12812	56929·6309	0·6794	−6·41	1·05	9·36	−0·27	1·60
11819	57291·6573	0·3789	−73·84	0·31	94·63	−1·03	1·26
12455	57292·6497	0·4439	−64·42	−0·36	82·61	−0·03	1·55
13032	57293·6905	0·5120	−51·71	−0·98	66·29	0·85	1·42
10972	57649·7896	0·8235	47·63	0·29	−61·05	0·01	0·98
8673	57942·9329	0·0138	139·27	0·40	−178·52	0·62	0·33
9658	57949·9838	0·4753	−59·08	−0·87	75·77	0·68	0·32
4545	57900·9241	0·2637	−79·11	0·87	101·32	−1·85	0·97
5286	57901·8892	0·3269	−79·13	0·36	101·47	−1·08	0·85
19234	58054·9081	0·3441	−78·10	−0·02	100·04	−0·69	0·60
9926	58390·6919	0·3257	−79·16	0·42	101·57	−1·08	0·90
10667	58747·8054	0·7036	0·83	0·52	2·10	2·50	0·39
10070	59478·8799	0·5624	−39·19	0·14	50·21	−0·53	0·86
8164	59820·8982	0·9522	119·99	1·79	−153·87	−1·40	0·60
8277	59821·8736	0·0160	139·34	0·78	−178·64	0·11	0·54
1335	59633·6570	0·6947	−4·15	−1·54	4·00	0·63	0·59
92	59589·6828	0·8160	43·09	−0·75	−55·25	1·31	0·35
11230	59864·9467	0·8357	52·68	−0·46	−67·54	1·01	0·58
11359	59865·9399	0·9008	88·06	0·19	−112·99	0·36	0·64
9581	59847·9677	0·7242	8·39	1·08	−10·81	−1·38	0·50
867	60004·6447	0·9809	133·93	1·26	−171·70	−0·56	0·37
5781	60131·8417	0·3077	−80·66	−0·12	103·33	−0·56	0·55
5061	60120·8407	0·5875	−33·94	−0·77	43·49	0·69	0·70
5152	60121·8515	0·6537	−15·34	−0·13	20·25	0·63	0·52
11220	60249·6464	0·0196	137·95	0·10	−176·86	0·98	0·74
11768	60271·8057	0·4702	−59·65	−0·45	76·45	0·08	0·52
11911	60272·8336	0·5375	−44·54	0·58	57·10	−1·11	0·56
10206	60222·7974	0·2619	−79·15	0·69	101·46	−1·54	0·07
10326	60223·8865	0·3332	−78·98	0·04	101·24	−0·69	0·48
1238	60432·9564	0·0197	138·27	0·45	−177·23	0·55	0·33
1356	60433·9744	0·0864	61·68	−0·27	−79·00	0·91	0·43
1650	60444·9462	0·8046	39·89	1·12	−51·19	−1·19	0·40
1733	60445·9598	0·8710	71·58	0·42	−91·79	0·01	0·33
3201	60503·8891	0·6632	−12·58	−0·19	16·61	0·64	1·34
5661	60556·7413	0·1231	0·53	−0·42	−1·37	−0·14	1·21
169	60686·6642	0·6284	−22·88	−0·49	29·45	0·56	0·69
1480	60721·6341	0·9176	98·62	0·84	−126·44	−0·31	0·74
4975	60859·9437	0·9719	129·58	0·93	−166·11	−0·16	0·75
6693	60900·9947	0·6592	−13·42	0·16	17·07	−0·45	0·74
7504	60928·9772	0·4910	−54·28	0·81	69·61	−1·46	0·77
7596	60930·0041	0·5583	−41·30	−0·98	53·04	1·03	0·80
8787	60970·8513	0·2323	−75·34	0·43	96·50	−1·25	0·70

(continued from previous page)

Summary and conclusions

We have presented a new spectroscopic orbit for NY Cep based on cross-correlation and spectrum disentangling. The latter also provided component line profiles for He I 667·8 nm and Hα. Combining that new solution for the helium line with older Reticon data has allowed us to estimate a provisional apsidal period of about 13500 yr. Further spectra should allow that period to be refined. Updated absolute dimensions and projected rotational velocities are also presented.

Acknowledgements

This study was based on observations obtained at the Dominion Astrophysical Observatory, Herzberg Astronomy and Astrophysics Research Centre, National Research Council of Canada.

The authors would like to thank the staff and directors of the Dominion Astrophysical Observatory for generous allocations of observing time over the many years during which this project took place. They would also like to thank the DAO technical staff for their set-up of and assistance with the telescope, spectrographs, and detectors. The authors are also grateful to an anonymous referee for comments which helped improve both the content and presentation of the paper.

References

(1) A. Tkachenko *et al.*, *A&A*, **683**, A252, 2024.
(2) S. Albrecht *et al.*, *AJ*, **726**, 68, 2011.
(3) Y. S. Ahn, *AP&SS*, **198**, 137, 1992.
(4) D. E. Holmgren *et al.*, *A&A*, **231**, 89, 1990.
(5) J. F. Heard & J. D. Fernie, in A. H. Batten & J. F. Heard (eds.), *Determination of Radial Velocities and Their Applications, Proceedings of IAU Symposium 30* (Academic Press), 1967, p. 219.
(6) J. Moffat, *J. RAS Can.*, **79**, 239, 1985.
(7) D. Tody, in D. L. Crawford (ed.), *Instrumentation in Astronomy VI, Society of Photo-Optical Instrumentation Engineers Conference Series*, **627** (SPIE), 1986, p. 733.
(8) D. Tody, in R. J. Hanisch, R. J. V. Brissenden & J. V. Barnes (eds.), *Astronomical Data Analysis Software and Systems II, Astronomical Society of the Pacific Conference Series*, **52** (ASP), 1993, p. 173.
(9) A. Coulais *et al.*, in Y. Mizumoto, K.-I. Morita & M. Ohishi (eds.), *Astronomical Data Analysis Software and Systems XIX, Astronomical Society of the Pacific Conference Series*, **434** (ASP), 2010, p. 187.
(10) W. B. Landsman, in R. J. Hanisch, R. J. V. Brissenden & J. V. Barnes (eds.), *Astronomical Data Analysis Software and Systems II, Astronomical Society of the Pacific Conference Series*, **52** (ASP), 1993, p. 246.
(11) J. Tonry & M. Davis, *Astronomical Journal*, **84**, 1511, 1979.
(12) I. E. Gordon *et al.*, *J. Quant. Spect. Rad. Trans.*, **277**, 107949, 2022.
(13) P. Hadrava, *A&ASS*, **114**, 393, 1995.
(14) P. Hadrava, *A&ASS*, **122**, 581, 1997.
(15) T. Sterne, *Proc. Natl. Acad. Sci.*, **27**, 175, 1941.
(16) R. W. Hilditch, *An Introduction to Close Binary Stars* (Cambridge University Press), 2001.
(17) K. F. Khaliullin & A. I. Khaliullina, *MNRAS*, **382**, 356, 2007.
(18) A. Palacios *et al.*, *A&A*, **516**, A13, 2010.
(19) A. Claret, *A&A*, **424**, 919, 2004.

REVIEWS

General Relativity: A Graduate Course, by Horaţiu Năstase (Cambridge University Press), 2025. Pp. 401, 29 × 18·5 cm. Price £18·5 (hardbound; ISBN 978 1 009 57575 1).

The author describes the mathematics in the book as "physics-friendly" and "not exaggerated in its use". While both might be true, it is one of the most mathematical books I've read. I assign it a relativity-book signature of 0+−++−.* The assumptions and lack of derivations

*The characters indicate maths-first or physics-first, breadth, depth, level, amount of maths, mathematical detail shown. With regard to the first, this book falls neatly into neither category. Although Chapter 2 provides some mathematical background, in general the necessary maths is introduced with each topic. Thus, the book